Research Article | Vol. 7, No. 9 | 1 Sep 2016 | BIOMEDICAL OPTICS EXPRESS 3345
Biomedical Optics EXPRESS

Optical coherence tomography endoscopic probe based on a tilted MEMS mirror

CAN DUAN,[1,4] QUENTIN TANGUY,[1,2] ANTONIO POZZI,[3] AND HUIKAI XIE[1,5]

[1]*Department of Electrical and Computer Engineering, University of Florida, Gainesville, FL, 32611, USA*
[2]*Department of Micro Nano Science and Systems, FEMTO-ST, Besançon, 25000, France*
[3]*Small Animal Surgery Clinic, University of Zurich, Zurich 8057, Switzerland*
[4]*cduan@ufl.edu*
[5]*hkx@ufl.edu*

Abstract: This paper reports a compact microendoscopic OCT probe with an outer diameter of only 2.7 mm. The small diameter is enabled by a novel 2-axis scanning MEMS mirror with a preset 45° tilted angle. The tilted MEMS mirror is directly integrated on a silicon optical bench (SiOB). The SiOB provides mechanical support and electrical wiring to the mirror plate via a set of bimorph flexure, enabling a compact probe mount design without the requirement of a 45° slope, which is capable to dramatically reduce the probe size and ease the assembly process. Additionally, the SiOB also provides trenches with properly-designed opening widths for automatic alignment of the MEMS mirror, GRIN lens and optical fiber. The 45°-tilted MEMS mirror plate is actuated by four electrothermal bimorph actuators. The packaged 2.7 mm-diameter probe offers 2-axis side-view optical scanning with a large optical scan range of 40° at a low drive voltage of 5.5 Vdc in both axes, allowing a lateral scan area of 2.2 mm × 2.2 mm at a 3 mm working distance. High-resolution 2D and 3D OCT images of the IR card, *ex vivo* imaging of meniscus specimens and rat brain slices, *in vivo* imaging of the human finger and nail have been obtained with a TDOCT system.

OCIS codes: (110.4500) Optical coherence tomography; (170.2150) Endoscopic imaging; (230.4685) Optical microelectromechanical devices; (170.3880) Medical and biological imaging.

References and links

1. D. Huang, E. A. Swanson, C. P. Lin, J. S. Schuman, W. G. Stinson, W. Chang, M. R. Hee, T. Flotte, K. Gregory, C. A. Puliafito, and et, "Optical coherence tomography," Science **254**(5035), 1178–1181 (1991).
2. C. W. Sun, S. Y. Lee, and K. F. Lin, "Review: Optical Scanning Probe for Optical Coherence Tomography," J. Med. Biol. Eng. **34**(1), 95–100 (2014).
3. B. J. Vakoc, D. Fukumura, R. K. Jain, and B. E. Bouma, "Cancer imaging by optical coherence tomography: preclinical progress and clinical potential," Nat. Rev. Cancer **12**(5), 363–368 (2012).
4. M. Atif, H. Ullah, M. Y. Hamza, and M. Ikram, "Catheters for optical coherence tomography," Laser Phys. Lett. **646**(9), 629 (2011).
5. P. H. Tran, D. S. Mukai, M. Brenner, and Z. Chen, "In vivo endoscopic optical coherence tomography by use of a rotational microelectromechanical system probe," Opt. Lett. **29**(11), 1236–1238 (2004).
6. P. R. Herz, Y. Chen, A. D. Aguirre, K. Schneider, P. Hsiung, J. G. Fujimoto, K. Madden, J. Schmitt, J. Goodnow, and C. Petersen, "Micromotor endoscope catheter for in vivo, ultrahigh-resolution optical coherence tomography," Opt. Lett. **29**(19), 2261–2263 (2004).
7. J. Su, J. Zhang, L. Yu, and Z. Chen, "In vivo three-dimensional microelectromechanical endoscopic swept source optical coherence tomography," Opt. Express **15**(16), 10390–10396 (2007).
8. M. J. Gora, J. S. Sauk, R. W. Carruth, K. A. Gallagher, M. J. Suter, N. S. Nishioka, L. E. Kava, M. Rosenberg, B. E. Bouma, and G. J. Tearney, "Tethered capsule endomicroscopy enables less invasive imaging of gastrointestinal tract microstructure," Nat. Med. **19**(2), 238–240 (2013).
9. X. Li, C. Chudoba, T. Ko, C. Pitris, and J. G. Fujimoto, "Imaging needle for optical coherence tomography," Opt. Lett. **25**(20), 1520–1522 (2000).
10. X. Liu, M. J. Cobb, Y. Chen, M. B. Kimmey, and X. Li, "Rapid-scanning forward-imaging miniature endoscope for real-time optical coherence tomography," Opt. Lett. **29**(15), 1763–1765 (2004).
11. Y. Wu, Y. Leng, J. Xi, and X. Li, "Scanning all-fiber-optic endomicroscopy system for 3D nonlinear optical imaging of biological tissues," Opt. Express **17**(10), 7907–7915 (2009).
12. L. Huo, J. Xi, Y. Wu, and X. Li, "Forward-viewing resonant fiber-optic scanning endoscope of appropriate scanning speed for 3D OCT imaging," Opt. Express **18**(14), 14375–14384 (2010).

#268736 http://dx.doi.org/10.1364/BOE.7.003345
Journal © 2016 Received 20 Jun 2016; revised 2 Aug 2016; accepted 3 Aug 2016; published 10 Aug 2016

Biomedical Optics EXPRESS

13. W. Jung, D. T. McCormick, J. Zhang, L. Wang, N. C. Tien, and Z. Chen, "Three-dimensional endoscopic optical coherence tomography by use of a two-axis microelectromechanical scanning mirror," Appl. Phys. Lett. **88**(16), 163901 (2006).
14. K. H. Kim, B. H. Park, G. N. Maguluri, T. W. Lee, F. J. Rogomentich, M. G. Bancu, B. E. Bouma, J. F. de Boer, and J. J. Bernstein, "Two-axis magnetically-driven MEMS scanning catheter for endoscopic high-speed optical coherence tomography," Opt. Express **15**(26), 18130–18140 (2007).
15. J. Sun, S. Guo, L. Wu, L. Liu, S. W. Choe, B. S. Sorg, and H. Xie, "3D in vivo optical coherence tomography based on a low-voltage, large-scan-range 2D MEMS mirror," Opt. Express **18**(12), 12065–12075 (2010).
16. K. H. Gilchrist, R. P. McNabb, J. A. Izatt, and S. Grego, "Piezoelectric scanning mirrors for endoscopic optical coherence tomography," J. Micromech. Microeng. **19**(9), 095012 (2009).
17. Y. Pan, H. Xie, and G. K. Fedder, "Endoscopic optical coherence tomography based on a microelectromechanical mirror," Opt. Lett. **26**(24), 1966–1968 (2001).
18. C. Duan, J. Sun, S. Samuelson, and H. Xie, "Probe alignment and design issues of microelectromechanical system based optical coherence tomography endoscopic imaging," Appl. Opt. **52**(26), 6589–6598 (2013).
19. S. R. Samuelson, L. Wu, J. Sun, S. W. Choe, B. S. Sorg, and H. Xie, "A 2.8-mm imaging probe based on a high-fill-factor MEMS mirror and wire-bonding-free packaging for endoscopic optical coherence tomography," J. Microelectromech. Syst. **21**(6), 1291–1302 (2012).
20. Y. Xu, J. Singh, C. S. Premachandran, A. Khairyanto, K. W. S. Chen, N. Chen, C. J. R. Sheppard, and M. Olivo, "Design and development of a 3D scanning MEMS OCT probe using a novel SiOB package assembly," J. Micromech. Microeng. **18**(12), 125005 (2008).
21. C. Duan, W. Wang, X. Zhang, J. Ding, Q. Chen, A. Pozzi, and H. Xie, "A 45°-tilted 2-axis scanning micromirror integrated on a silicon optical bench for 3D endoscopic optical imaging," in *28th IEEE International Conference on Micro Electro Mechanical Systems (MEMS)* (IEEE, 2015), pp. 948–951.
22. C. Duan, Q. Tanguy, A. Pozzi, and H. Xie, "An Optical Coherence Tomography Endoscopic Probe Based on a Tilted MEMS Mirror," in *Biomedical Optics* (OSA, 2016), pp. JW3A.17.

1. Introduction

Optical coherence tomography (OCT) is a powerful biomedical imaging technique for real-time, cross-sectional imaging with 1-10 μm resolution and 1-3 mm imaging depth [1]. In recent years, OCT has been widely investigated in the area of endoscopic imaging of internal organs for cancer screening and early cancer diagnosis [2–4]. A variety of OCT probes and catheters have been developed to facilitate endoscopic OCT imaging with various optical scanning mechanisms such as using an external motor to spin an optical fiber with a prism attached [5–7], a rotary joint to rotate and linearly translate a fiber [8,9], a piezoelectric tube to tether a fiber [10–12], or a micromirror to scan the optical beam in free space at the distal end of a fiber [13–15]. Among them, MEMS micromirrors offer a more promising solution for rapid 3D endoscopic OCT imaging due to their small size, fast scanning speed and 2-axis linear scan capability. Several side-viewing and forward-viewing endoscopic OCT probes have been demonstrated in the last two decades using MEMS mirrors based on electrostatic [13], electromagnetic [14], piezoelectric [16] and electrothermal [17] actuation mechanisms. However, further minimization of MEMS micromirror enabled endoscopic OCT probes still remains a primary challenge due to the complexity of designing small probe mounts and the difficulty of assembling small probes in narrow space.

Several types of planar electrothermal MEMS mirrors with 1-axis or 2-axis scan capability have been extensively employed in side-viewing endoscopic OCT probes [15,17–19]. A typical side-viewing endoscopic OCT probe is shown in Fig. 1(a) [19], where a planar MEMS micromirror chip is mounted on a 45° sloped ferrule inside the probe body to direct an optical beam to one side of the probe. To assemble the probe, a flexible PCB (FPCB) is first glued on the slope. Then the MEMS chip is stacked on the FPCB using silver epoxy or instant glue; this step is tedious as the MEMS chip is very small and the housing space is very limited. The 45° slope takes extra space which increases both the probe size and the probe fabrication cost. The electrical connection is provided either by wire bonding [15] or flip-chip bonding [19]. Wire bonding further increases the probe size while flip-chip bonding may pose a risk of high electrical contact failure rate. The failure rate of electrical connection is high for flip-chip bonding because the pads on the small MEMS mirror chip must be aligned with the pads on the FPCB in a very small space. Silver epoxy is manually placed on the pads, so the contact areas and strengths are not uniform, easily causing broken circuits or short circuits.

Biomedical Optics EXPRESS

Another popular side-viewing probe design was demonstrated by Xu *et al*. [20], employing a SiOB with a pre-fabricated trench to hold a micromirror vertically. The micromirror was dropped into the trench and fixed manually, and the electrical connections between the MEMS actuators and the embedded metal paths on the SiOB were provided with solder balls [20]. But to form reliable electrical and mechanical connections is still a challenge due to significant deformation of the solder balls during reflow and curing.

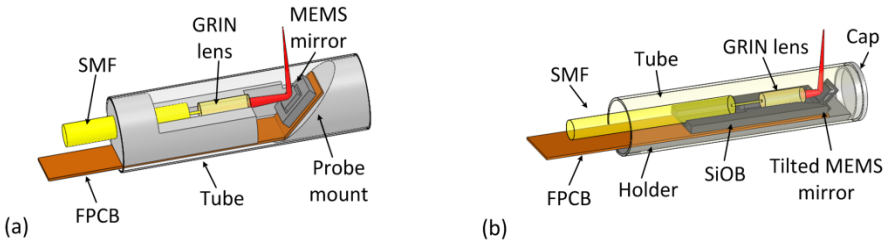

Fig. 1. (a) Illustration of the probe design with the MEMS mirror fixed on a 45° slope. (b) The new probe design with the MEMS mirror tilted 45° out of plane.

In this paper, we report a compact OCT probe (Fig. 1(b)) with a simplified probe mount design and simplified assembly process. This probe is enabled by a novel MEMS micromirror design with the mirror plate tilted at a preset 45° and integrated on a SiOB [21]. The tilted MEMS mirror simplifies the probe mount design by eliminating the need of a 45° slope or pocket to fix a planar MEMS mirror as in prior work [15,19]. Furthermore, the SiOB, which contains large pads connected to the actuators, enables easy and stable electrical connection. In this paper, the MEMS mirror will be introduced first, followed by the probe design, the probe assembling, and the imaging experiment results.

2. The 45° tilted MEMS mirror

The 3D model of the employed 45° tilted MEMS mirror is shown in Fig. 2(a), consisting of a 2-axis scanning single-crystal-silicon (SCS) mirror plate tilted out of the surface of a SiOB. The 45° tilt of the mirror plate is achieved with the initial bending of a set of flexure bimorph cantilevers and the stopping by a stopper structure anchored on the SiOB. The flexure bimorph consists of SiO_2 as the top layer and Al as the bottom layer, which bends towards the SiOB upon releasing. The tilt angle can be precisely controlled by properly choosing the flexure bimorph length and the distance from the mirror frame to the silicon sidewall [21]. The SiOB provides mechanical support and electrical wiring to the bimorph actuators as well as trenches for fixation and optical alignment of the optical components.

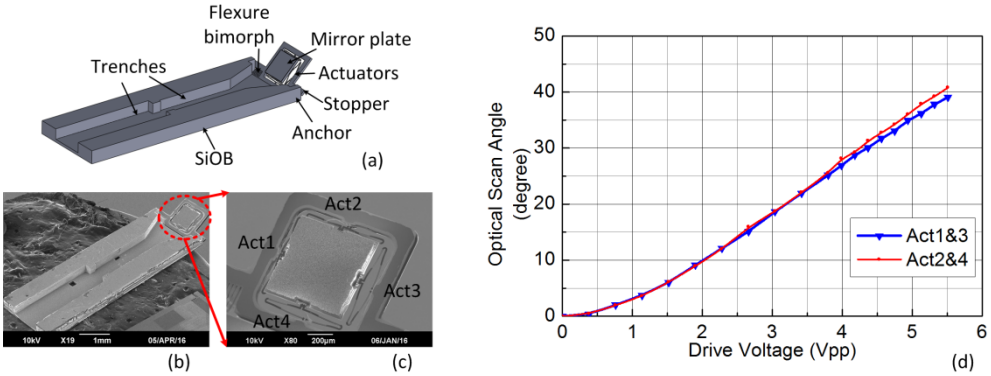

Fig. 2. The 45° tilted MEMS mirror with long SiOB. (a) 3D model. (b) SEM of a fabricated device. (c) A close-up SEM of the mirror plate with four actuators. (d) Scan angle versus applied voltage.

Biomedical Optics EXPRESS

Figures 2(b) and 2(c) show two SEMs of a fabricated 45° tilted MEMS mirror. The fabricated device has a footprint of 2.22 mm × 6.78 mm and a height of 0.85 mm, and the mirror plate is 0.72 mm × 0.72 mm in size and tilted by 63°, which is not exactly 45° due to the silicon sidewall undercut during the device release. The maximum total optical scan angle of the mirror plate is around 40° at 5.5 Vdc for both axes, as shown in Fig. 2(d). The first mechanical resonance peak of the mirror plate for the tip-tilt scanning mode in both directions is approximately 750 Hz. More details about the design, fabrication and characterization of this MEMS mirror can be found in [21].

3. Probe design

The schematic of the side-viewing OCT probe design based on the 45° tilted MEMS mirror is shown in Fig. 1(b). The side-viewing probe is defined by five main components: a MEMS chip, a GRIN lens, a single mode fiber (SMF), an FPCB and a probe mount. The MEMS chip consists of a 45° tilted MEMS mirror and a SiOB and is mounted on the FPCB for electrical connections using a wire-bonding-free packaging technique. The GRIN lens and SMF are placed in the trenches on the SiOB. The trenches are designed with proper dimensions to ensure good optical alignment of the optical components. The MEMS-FPCB module is fixed on a 25 mm-long, 2.3 mm-wide and a 0.95 mm-thick flat holder and inserted into a glass tube with an outer diameter of 2.7 mm. The flat holder is made using 3D printing, so the cost is very low compared to the prior probe design shown in Fig. 1(a) [19].

The optical design of the probe with light ray tracing is shown in Fig. 3. An SMF fiber (SMF-28, Corning) with an 8° cleaved fiber tip is connected to the sample arm of an OCT system to deliver a broadband light with a center wavelength of 1310 nm. The outer diameter of the SMF is 0.9 mm and the 8° cleaved fiber tip helps to reduce back-reflection light. The fiber tip is optically aligned with and physically fixed at the end of a GRIN lens. Optical UV glue (NOA 61, Norland Optical Adhesives) with a refractive index of 1.542 at 1310 nm is used to fix the fiber tip with the GRIN lens and provide refractive index matching. The distance between the fiber tip and the GRIN lens has a significant effect on the lateral resolution and the working distance of the probe. With a larger fiber tip-lens distance, the lateral resolution will be enhanced while the working distance will be decreased. The fiber tip-lens distance should be controlled within 0.1 mm to obtain the working distance larger than 3.5 mm and lateral resolution of around 25 μm [18]. The GRIN lens (ILW-070, GoFoton, NJ) employed has a pitch of 0.27 with a length of 1.955 mm, a diameter of 0.7 mm and a focal length of 5 mm. A 45° tilted MEMS mirror is placed at the distal end of the flat holder, and the height of the mirror center is around 0.52 mm, as shown in Fig. 3. The mirror center is aligned with the optical axis, and the mirror plate is 45° to the incident light beam. The distance between the GRIN lens and the mirror plate center is designed as 1 mm to achieve a working distance of 3 mm with a lateral resolution around 20 μm in air. The effects of the distance between the fiber and GRIN lens, the curvature of the MEMS mirror plate and the cylindrical tubing can be found in [18].

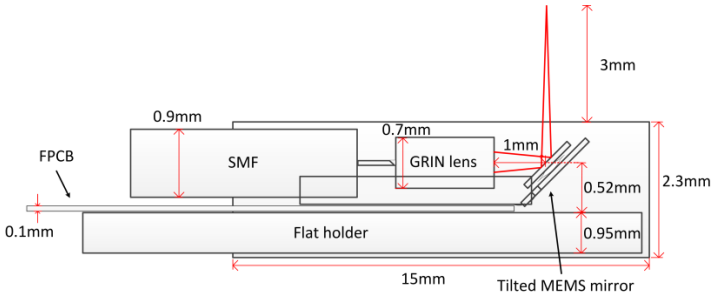

Fig. 3. Optical design of the side-viewing endoscopic OCT probe employing the tilted MEMS mirror (not drawn to scale).

Biomedical Optics EXPRESS

Electrical connections to the four actuators of the MEMS mirror are required. An FPCB shown in Figs. 4(a) and 4(b) is used to achieve compactness while maintaining stable electrical connections. The width of the PCB is 2.25 mm, and the length is 40 mm. There are five Al-coated bonding pads on the back side of the SiOB, as shown in Fig. 4(c), and there are five exactly matched bonding pads at one end of the FPCB, as shown in Fig. 4(b). Several markers are placed on the FPCB to facilitate the alignment of the SiOB to the FPCB. The length of the SiOB is designed such that large pad size and large spacing between the pads are allowed. Thus, the MEMS chip can be directly flip-chip bonded on the FPCB without the need for wire bonding. This wire-bonding-free technique leads to reliable electrical connection and small form factor. As shown in Fig. 4(c), the size of each pad is around 1 mm × 0.6 mm and the spacing between any two pads is greater than 1 mm, which is large enough for easy assembly and to ensure reliable electrical connections as well. The other end of the FPCB has five corresponding solder pads which are soldered with five copper wires to carry four drive signals and one electrical ground. Compared to a side-viewing probe design using a planar MEMS mirror, a 45° slope or pocket or a separate SiOB with a trench for mounting the MEMS mirror is not needed in this new probe design. Only a strip with a flat surface is utilized to hold the tilted MEMS mirror, which significantly reduces the volume of the whole probe and decreases the fabrication cost of the probe mount.

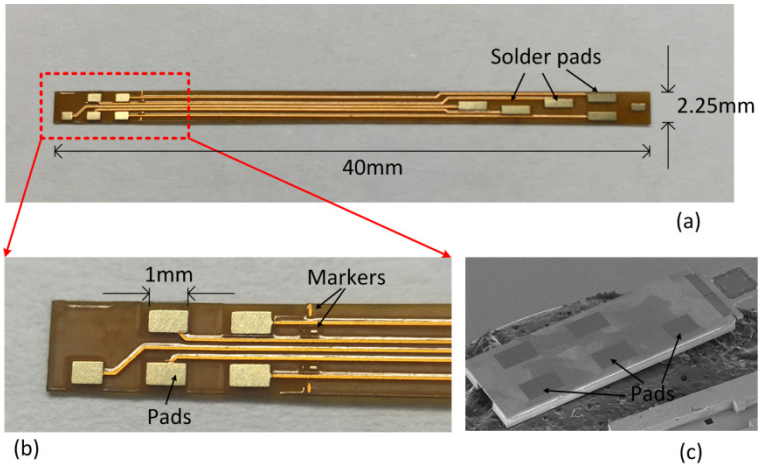

Fig. 4. Wire-bonding-free technique for 45° tilted MEMS mirror by using FPCB. (a) and (b) Photographs of FPCB. (c) SEM of the conductive pads on the backside of a SiOB.

4. Probe assembly

An endoscopic probe prototype has been assembled using the fabricated tilted MEMS mirror and other optical components. Five copper wires are first soldered on one FPCB as shown in Fig. 4(a), and then the FPCB with the copper wires is attached to a 3D printed flat strip using an instant glue. After that, a small amount of electrically conductive silver epoxy (EMS #12642-14, Electron Microscopy Sciences) is dispensed on each pad of the FPCB. Next, the MEMS micromirror chip is flipped over and pressed on the FPCB with the edges of the SiOB aligned to the corresponding markers on the FPCB to ensure proper and reliable electrical connections. The silver epoxy can be cured in 4 hours at room temperature to achieve good mechanical and electrical connections. A GRIN lens and an SMF are glued inside the trenches on the SiOB using an optical glue, and they are aligned automatically to the center of the MEMS mirror plate. The mirror plate is tilted 45° initially with respect to the incident light beam. The auto-alignment is realized by carefully designing opening widths of the trenches on SiOB in order to keep the optical axes of the fiber and the GRIN lens aligned with the center height of the mirror plate. The auto-alignment eliminates the difficulty in manual

Biomedical Optics EXPRESS

adjustment and assembly. A transparent glass tube is then slid from the distal end of the probe for protection and can be replaced by other tubes or imaging windows made of any biocompatible and transparent material. A cap can be added and fixed using glue at the end of the probe head to encapsulate the probe.

Figure 5(a) shows a fully packaged endoscopic OCT probe, composed of a probe head, an SMF fiber, and several copper wires. As shown in Fig. 5(b), the outer diameter of the probe is 2.7 mm and can be decreased by minimizing the wall thickness of the tubing. The inner diameter of the prototype is 2.3 mm. This tilted MEMS mirror design can be modified such that the width of the SiOB is reduced to the same width of 1.2 mm as that of the tilted mirror, which will enable the further miniaturization of the endoscopic OCT probe. An enlarged photograph of the probe head is shown in Fig. 5(c), indicating that the 45° tilted MEMS mirror is attached both physically and electronically on a flat holder.

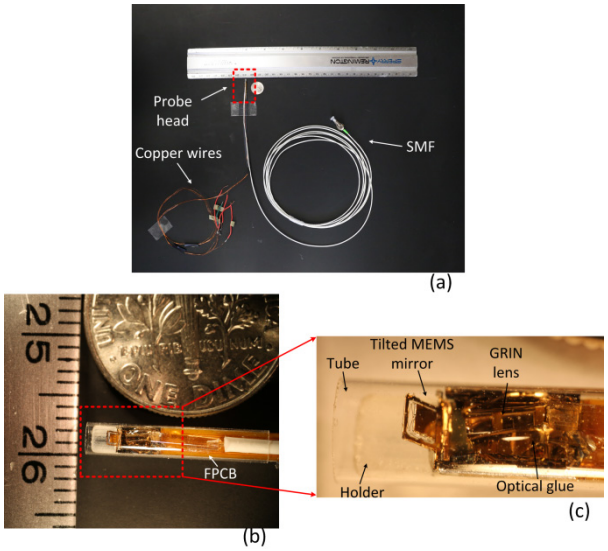

Fig. 5. Photographs of the side-viewing endoscopic probe. (a) Overview of the packaged probe. (b) Fully packaged probe placed beside a ruler and one dime. (c) Close-up of the probe head.

Figure 6(a) shows a packaged probe head with a red light delivered to the mirror plate through the SMF and GRIN lens. A semiconductor laser with a wavelength of 650 nm was used for demonstration and measurement. The longitudinal scan pattern with the drive voltage of 3 Vpp is shown in Fig. 6(b). The total optical scan angle was measured to be 18.6° in this image. In both axes, the maximum scan angle of 40° can be achieved with a maximum drive voltage of 5.5 Vdc.

Biomedical Optics EXPRESS

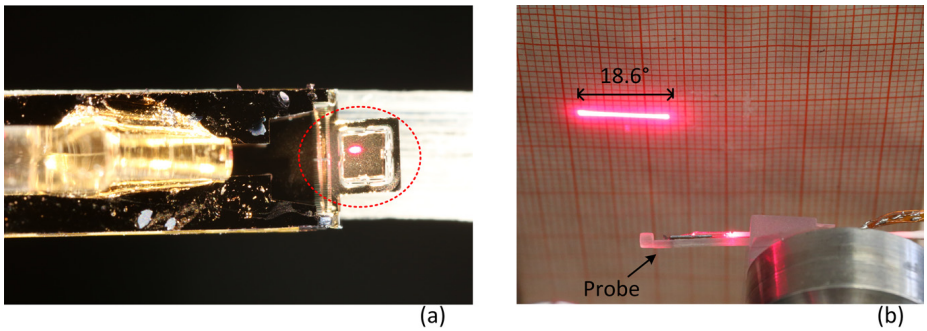

Fig. 6. Photographs of the packaged probe head without tubing. (a) A packaged probe. (b) One-axis scan pattern with driven voltage of 3V for opposed actuators in the longitudinal direction.

5. OCT imaging experiments

5.1 Imaging characterization

The imaging performance of the probe is demonstrated using a TDOCT system, shown in Fig. 7. The broadband light source (Denselight, DL-BX9-CS3159A) has a center wavelength of 1310 nm and an FWHM of 75 nm. As shown in Fig. 7(a), the probe is connected to the sample arm of the TDOCT system to provide a 2D lateral scan on a sample. As shown in Fig. 7(b), the sample is placed in a glass holder which is placed on top of the probe and the light exiting the side-viewing probe scans the sample from the bottom side. The MEMS mirror inside the probe is capable of providing a raster scan with the fast scan of 1.25 Hz and the slow scan of 0.005 Hz. A series of cross-sectional 2D images can be obtained in real time, and 3D rendering can be achieved by stacking the 2D images. The lateral scan speed of the MEMS mirror can be increased, but it is limited by the axial scan speed (500 Hz) of the TDOCT system. The axial resolution is 10 μm, which is determined by the line-width of the broadband light source; the lateral resolution is measured to be approximately 23 μm with the same broadband source, which is a compromise of the 3 mm imaging depth.

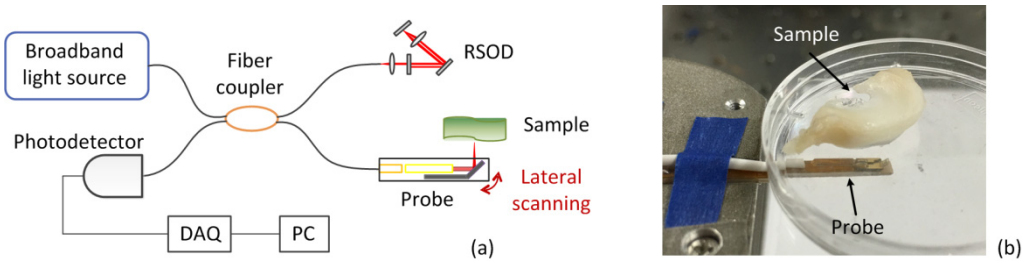

Fig. 7. MEMS based OCT imaging probe. (a) Schematic of a TDOCT system using an endoscopic OCT probe as the sample arm. (b) Photograph of the side-viewing probe connected to the OCT system.

The lateral scan range at a working distance of 3 mm was measured by imaging a printed customized calibration pattern with a 0.1 inch or 2.54 mm pitch, as shown in Fig. 8(a). The ratio of the black area to the area of one unit is 95%. OCT images of the black area on the printed pattern are shown as shallow bright lines (indicated by the stars), while the imaging depth of the white lines is larger, as indicated by the arrows in Figs. 8(b) to 8(e). The scan range or the image width can be determined by the ratio of the total pixel number and the pixel number between the two longer bright lines (Fig. 8(b)), which indicate the space between the adjacent white patterns. If there is only one grid space shown in the image, which means the image width is smaller than 2.54 mm, the scan range can be determined by recording the displacement of the printed calibration pattern when the space moves from the

Biomedical Optics EXPRESS

left to right side of the imaging window, shown in Figs. 8(c) to 8(e). The lateral displacement was generated by manually moving the translational stage that held the sample. The measured width of the 2D OCT images is 1.75 mm at the working distance of 3 mm, and the height of the 2D OCT images is 2.5 mm. The corresponding optical scan angle of the probe is ± 16.3° in the transverse direction when applying a 5 V drive voltage.

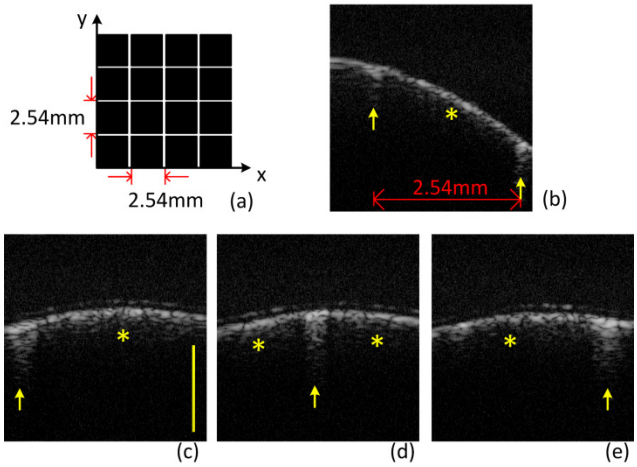

Fig. 8. Characterization of the lateral scan range of the side-viewing probe. (a) The calibration pattern with a grid size of 2.54 mm. Cross-sectional OCT images of the printed calibration pattern: (b) driving a single actuator to scan in the x-direction; (c) to (e) driving a pair of opposing actuators in the y-direction with the translational stage at different positions.

5.2 OCT imaging results

OCT images of an IR card, a human finger, a human nail, rat brain tissue slices, and canine menisci samples have been obtained using the OCT probe prototype in combination with the TDOCT system. Figure 9 shows a series of 2D OCT images obtained by the endoscopic OCT probe. Different layers of the samples are clearly observed in the real-time 2D OCT images. Figure 9(a) shows the cross-sectional OCT image of an IR card. The top two bright lines represent the surface of the glass holder and the plastic layer of the IR card surface respectively. The penetration depth is measured to be around 0.7 mm inside the IR card. Figure 9(b) represents both the epidermis and dermis layer as well as some sweat ducts beneath the surface of the human finger. And Fig. 9(c) shows the cross-sectional of a human nail with the imaging depth of 1.3 mm. The lunula layer was clearly delineated. In Fig. 9(c), only the right part of the image shows the presence of the lunula and the left part does not contain this layer since this cross-sectional image was taken at the interface of the normal nail area and the lunula area. The fluctuations of the nail surface were introduced by the moving finger, which can be eliminated by using an SSOCT system with a much higher imaging speed. 2D OCT images of rat brain tissue slices have also been obtained. The thickness of the rat brain tissue was measured to be 0.6 mm, as shown in Fig. 9(d). The white matter and the gray matter show different scattering properties (Fig. 9(e)) as the white matter appeared brighter than the gray matter in the OCT images. Some nerve fibers or axons were also observed as bright dots in the region of the corpus callosum, as shown in Fig. 9(f).

Biomedical Optics EXPRESS

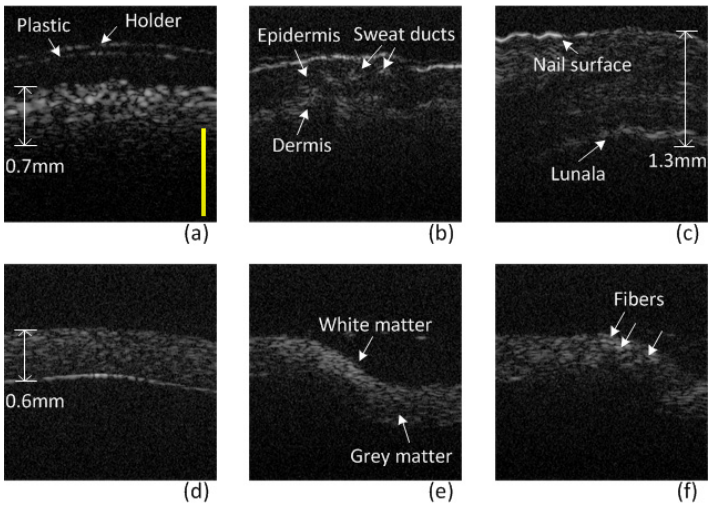

Fig. 9. OCT imaging performance of the side-viewing probe. 2D OCT images of (a) IR card, (b) human finger, (c) human nail, and (d) to (f) rat brain tissue slice.

3D OCT renderings of the brain tissue slices were obtained by stacking a series of 2D OCT images, as shown in Figs. 10(a) to 10(d). The 3D images were achieved by scanning the sample in two orthogonal directions with a fast scan frequency of 1.25 Hz and a slow scan frequency of 0.005 Hz, respectively. Two stainless steel balls with different diameters were placed on top of a thin slice of a rat brain tissue. The interfaces between the balls and the brain tissue were clearly delineated by the bright curves shown in Figs. 10(a) and 10(c). The 3D images in Figs. 10(b) and 10(d) provide better views of the brain tissue slice with the ball placed on top of it. Deformation of the brain tissue generated by the weight of the stainless ball was observed. The deformation varies with the ball size, providing a potential method to study the refractive index change of the brain tissue due to mechanical deformation or stress.

Figures 10(e) and 10(g) are 2D OCT images of a normal canine meniscus and a canine meniscus with a horizontal meniscal tear created by a single incision, respectively. The lesion was filled with a fat gel, shown as a dark gap inside the meniscus in the OCT image (Fig. 10(g)) due to the lower scattering of the gel compared to the meniscus tissue. The outline of the meniscal tear was clearly delineated in Fig. 10(g). A 3D image of the canine meniscus with the horizontal tear is shown in Fig. 10(h). It is capable of facilitating the diagnosis of meniscal tears *in vivo* with the MEMS-based endoscopic OCT probe integrated within the traditional arthroscope.

The above experiments show that the tilted MEMS mirror functions properly in an endoscopic probe for OCT imaging. This tilted MEMS simplifies the mechanical design and thus can drastically reduce the cost and enable even smaller probes. On the other hand, as a TDOCT system is employed, the imaging speed is limited to a few frames per second by the scanning speed of the galvanometer in the rapid scanning optical delay line (RSOD). And the resolution is also limited by the relatively small line-width of the employed broadband light source. A swept source OCT system will be used in the future to overcome these limitations.

Biomedical Optics EXPRESS

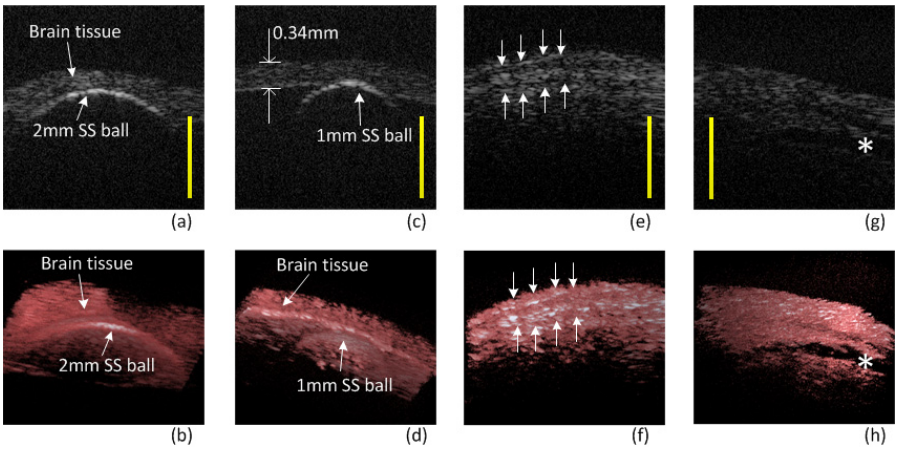

Fig. 10. 2D and 3D OCT images obtained by the endoscopic probe. (a) 2D and (b) 3D OCT images of a rat brain tissue slice with a stainless steel ball of 2 mm in diameter. (c) 2D and (d) 3D OCT images of a rat brain tissue slice with a stainless steel ball of 1 mm in diameter. (e) 2D and (f) 3D OCT images of the normal canine meniscus. (g) 2D and (h) 3D OCT image of the canine meniscus with a simulated horizontal meniscal tear.

6. Summary

In this work, we have developed a miniaturized endoscopic side-viewing OCT probe using a tilted 2-axis MEMS mirror for *in vivo* 3D imaging of biological specimens. The endoscopic OCT probe has an inner diameter of 2.3 mm and an outer diameter of 2.7 mm. It possesses the advantages of simplified probe mount design, reduced probe size and more stable electrical connections compared to the planar MEMS mirrors based endoscopic OCT probes. The flat strip holding the FPCB and MEMS can be created by 3D printing, resulting in low cost. The large pad spacing allowed by the SiOB makes the assembly much easier and the electrical connection much more reliable. Also, the trenches and markers on the SiOB enable quick optical alignment. High-resolution imaging capability of the probe has been demonstrated using a TDOCT system on IR cards, biological specimen and human fingers and nails. The imaging results indicate that the probe is promising for real-time *in vivo* imaging of the epithelial layers of internal organs with micrometer-resolution, which is attractive for the early cancer detection and the image-guided surgery. The tilt angle of the mirror plate of the fabricated devices was about 63°. This deviation from the designed 45° tilt angle resulted from the silicon undercut during the DRIE release steps. Fortunately the OCT imaging has large tolerance to the initial tilt angle. This is evidenced by the OCT imaging experiments reported in this paper which were all performed with the 63°-tilted MEMS mirrors. Furthermore, the 45° tilt angle can be easily achieved by extending the length of the anchor on the SiOB. In the future, narrower SiOB will be used so that the width of the MEMS chip will be less than 1.2 mm. Consequently, the probe size can be further reduced to below 2.0 mm, allowing even broader applications inside human body including intravascular imaging.

Acknowledgments

Portions of this work were presented at the Biomedical Optics Congress in 2016, JW3A-17 [22].

Funding

National Science Foundation (NSF) (1002209, 1512531).